



Machining properties of as-built additive manufactured Ti6Al4V titanium alloy through selective laser melting: a comprehensive investigation

Surinder Pal¹ · Xavier Velay¹ · Waqas Saleem²

Received: 29 February 2024 / Accepted: 5 August 2024 / Published online: 13 August 2024
© The Author(s), under exclusive licence to Springer-Verlag London Ltd., part of Springer Nature 2024

Abstract

Over the past two decades, additive manufacturing (AM) has gained attention for its numerous benefits. Despite the growing interest in AM processes for as built Ti6Al4V alloys, there is a lack of comprehensive benchmark research on their impacts. This study addresses this gap by conducting a thorough standard comparison encompassing microstructure, cutting speed, chip analysis, surface roughness, and hardness. Additionally, a conventionally processed Ti6Al4V (grade 23) alloy is a reference for thorough comparison. The research outcomes contribute to a better understanding of AM techniques' implications on building selective laser melted (SLM) Ti6Al4V alloys. Specifically, SLM Ti6Al4V grade 23's investigated material, demonstrates lower cutting forces. This observation is attributed to inherent characteristics, including porosity and the presence of unmelted particles resulting from the SLM process. Particularly, remarkable is the substantially higher hardness observed in SLM Ti6Al4V compared to its conventionally processed counterpart. This insight not only underscores the distinctive attributes of the material but also provides valuable knowledge for optimizing the application of AM Ti6Al4V alloy.

Keywords AM · Ti6Al4V · Cutting speed · SLM · Machining

1 Introduction

Among the spectrum of additive manufacturing technologies, SLM has emerged as an and up-and-coming method for fabricating metallic components in critical industries such as aerospace and biomedical engineering. This is attributed to its inherent capacity to construct intricate parts with complex geometries and significantly reduce lead times, thus contributing to the advancement of these fields. This makes them particularly relevant for inclusion in research papers focusing on these fields [1–3]. Additionally, the growing AM technology further enhances the significance of titanium alloys in research. Researchers and manufacturing industries have drawn the attention of researchers and manufacturing industries to AM due to its advantageous features, including freedom of design, on-demand manufacturing, minimized raw material waste,

and low energy consumption [4]. AM, a method of layer-wise material production, allows for design flexibility and the fabrication of intricate internal structures, challenging or unattainable through traditional processing methods [5]. SLM a prominent AM technology, has witnessed a significant rise in global usage. The exceptional capabilities of SLM contribute to its increasing prominence in the field [6–8]. It has been observed that components made from the SLM process using Ti-6Al-4 V exhibit higher tensile strength, yield strength, and hardness when compared to their conventional counterparts [9, 10]. Murr et al. [11] have attributed the high strength and hardness of SLM Ti-6Al-4 V to the presence of martensite phase regimes in its microstructure. Nevertheless, the unfavorable issues of inadequate surface morphology, elevated surface roughness parameters, and deviations from specified dimensional accuracy significantly impede the extensive utilization of AM parts [12–14]. Consequently, to address the challenges related to the surface finish and geometric tolerances of AM parts, the implementation of secondary subtractive finishing operations becomes imperative to attain high-quality products suitable for precision engineering applications [13, 15]. To address these limitations, post-finishing machining of additively manufactured components becomes essential to ensure

✉ Surinder Pal
surinder92.pal@gmail.com

¹ Mechanical & Manufacturing Engineering Department,
Atlantic Technological University, Sligo, Ireland

² Technological University Dublin, Dublin, Ireland

product quality and adherence to tolerance limits. Wang et al. [16] stated that in contrast to conventional subtractive machining methods like turning, milling, and grinding, the innovative AM technology offers distinct and notable advantages. This includes creating components with intricate geometric structures, swift prototyping, and facilitating of functional design [17]. Montevecchi et al. [18] explored the cutting force behavior of two additive manufacturing technologies, laser deposition, and wire arc additive manufacturing components manufactured through SLM [19–21]. This is notable considering the substantial enhancements that machining could offer regarding surface integrity and performance for SLM-produced parts. Similarly, Wysocki et al. [22] suggested that AM titanium alloy exhibited superior mechanical properties compared to numerous conventional methods. Nevertheless, there remains a need for enhancements in the surface quality of AM titanium alloys. Duro et al. [23] demonstrated the ability of SLM to fabricate intricate parts in their as-built or nearly finished forms, requiring minimal machining for them to be commissioned. Furthermore, Brinksmeier et al. [24] exhibited the presence of unmelted powder particles and laser scan marks on the surfaces of SLM-produced parts leading to suboptimal surface finish and dimensional accuracy, impacting their functional performance. Consequently, post-machining becomes essential to attain the required accuracy and tolerance levels. Inadequate literature is available discussing the machinability of additively manufactured titanium alloys, with only a limited number of papers addressing this topic [19, 25–27]. Therefore, to address these limitations, post-finishing machining of additively manufactured components becomes essential to ensure product quality and adherence to tolerance limits. This research conducted a comprehensive comparative study involving milling machining on SLM fabricated and conventional Ti6Al4V. The investigation focused on comparing cutting forces, chip section, and hardness. Initial results indicate distinctive mechanical behaviors in terms of cutting forces and hardness. Further analysis is underway to delve deeper into the observed differences, providing valuable insights into the comparative performance of Ti6Al4V components manufactured via SLM and conventional processes. This study contributes to understanding material properties and machining characteristics, aiding advancements in Titanium Alloy Component fabrication. These findings advance our understanding of SLM Ti6Al4V, promoting its use in applications requiring high strength, precision, and wear resistance. This research supports the reduction of machining costs, improvement of product quality, and enhancement of performance in high-demand industries such as aerospace, medical implants,

tooling, and precision engineering. It is crucial for optimizing post-finishing machining processes and improving product quality in critical applications.

2 Experimental method

2.1 Powder and SLM parameters

The Ti6Al4V Grade 23 was manufactured using powder with a particle size ranging from 23 μm , sourced from AP&C Powder Metallurgy, Canada. The chemical composition of Ti6Al4V Grade 23, analyzed by ASTM E29, is detailed in Table 1. A total of 3 samples were fabricated as the dimensions of 20 \times 20 \times 20 mm cube. To create these samples for machining, the “EOS M 280 Metal Print” was employed, equipped with a solid-state laser of 200 watts within a setting of inert gas (specifically argon). The SLM parameters used in this analysis are summarized in Table 2. The fabricated components were meticulously separated from the substrate using a wire electrical discharge machining (wire-EDM) machine.

$$E_v = \frac{P}{v \cdot h \cdot t} \quad (1)$$

Concerning the parameters within the ongoing process, an equation referred to as the volumetric energy density (1) is employed to analyze the impact of various process parameters in SLM processing. This equation defines the average applied energy per unit volume of material. It includes distinct variables: P representing laser power, h indicating hatch distance, v denoting scanning velocity, and t signifying powder layer thickness [6]. Figure 1 displays images of the Ti6Al4V samples produced by the “EOS M 280 Metal Print” machine, at the South-Eastern Applied Materials Research Centre in Ireland. Table 2 delineates the powder material composition employed in Ti6Al4V fabrication, per ASTM F3001-14 specifications. Additionally, Table 3 presents the chemical composition of the Conventional Ti6Al4V utilized in the study.

Table 2 Used process parameters to fabricate SLM samples

Layer scan speed	Hatch spacing	Overlap	Laser power	Layer thickness
1250 mm/s	115 μm	30%	200W	30 μm

Table 1 Chemical composition of used Ti6Al4V Grade 23 powder

Item	Al	V	Fe	O	C	N	H	Y	Ti
Wt. %	6.41	3.93	0.21	0.08	0.01	0.03	0.002	<0.40	Balance

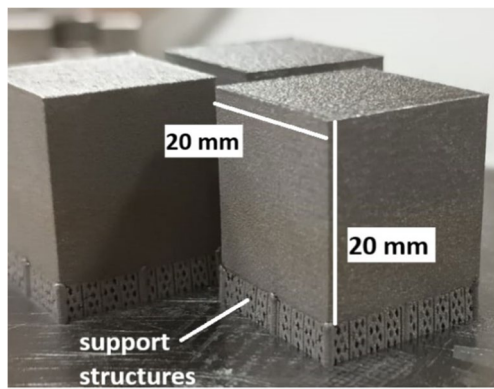


Fig. 1 Build in SLM samples

2.2 Materials used for testing

This study employed two varieties of titanium alloys of grade 23: conventional Ti-6Al-4 V and SLM as built Ti-6Al-4 V. Both materials were shaped into cubes with each side measuring 20 mm. The material samples and dimensions are illustrated in Fig. 2. The microstructure of both work materials is depicted in Fig. 3. Tables 1 and 2 present the chemical composition and mechanical properties of the materials utilized in this research, respectively.

Fig. 2 a Material samples of Ti6Al4V (Conventional & AS build SLM) and b CAD model

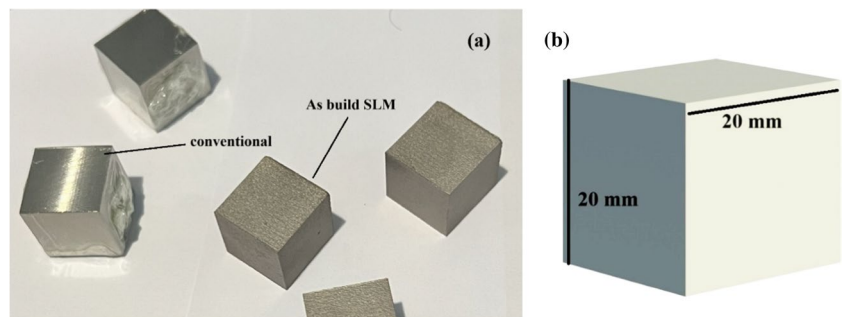
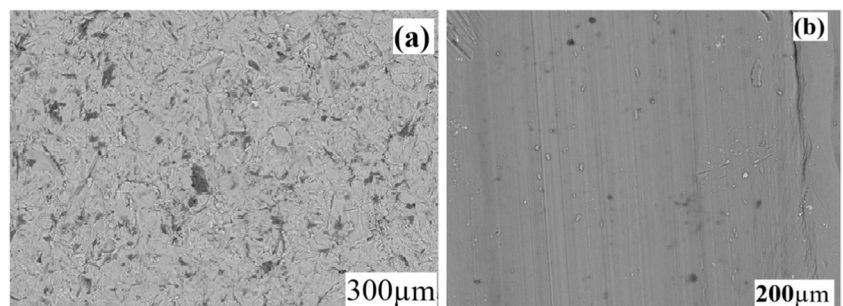


Table 3 Chemical composition of the used conventional Ti6Al4V

Item	Al	Fe	V	N	O	H	C	Ti
Wt. %	6.84	0.17	4.37	0.03	0.20	-	0.08	Bal

Fig. 3 Microstructure of a as build SLM Ti-6Al-4 V and b conventional Ti-6Al-4 V



2.3 Characterization

Brinksmeier and several other researchers emphasize that the presence of unmelted powder particles and laser scan marks on surfaces in SLM-produced parts leads to compromised surface finish and dimensional accuracy. This, in turn, directly affects the functional performance of these components [23, 24]. An illustration of unmelted particles on the underside of the sample is provided in Fig. 4, while Fig. 5 showcases identified porosity within the sample. Additionally, the microstructure of SLM components is shaped by the laser scan vectors and the direction of the building process. The build process’s high-temperature gradients form a fully transformed α' martensitic phase [28]. The microstructures of $\alpha + \beta$ titanium alloys, such as Ti-6Al-4 V, produced via both AM and conventional methods, are varied and significantly impact their mechanical properties [29, 30]. The Widmanstätten microstructure, commonly seen in these alloys, is defined by its acicular α phase interwoven within a β matrix, which can enhance strength but potentially reduce ductility. In contrast, the duplex microstructure, which comprises a mix of primary α grains within a transformed β matrix, offers a balanced combination of strength and ductility, making it suitable for various applications [31]. The basket-weave microstructure features interlocking α laths within a

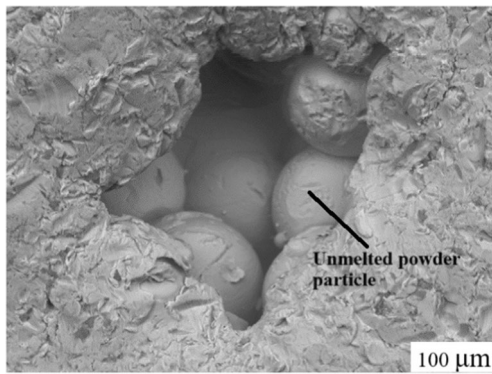


Fig. 4 Unmelted particle of as build SLM Ti6Al4V

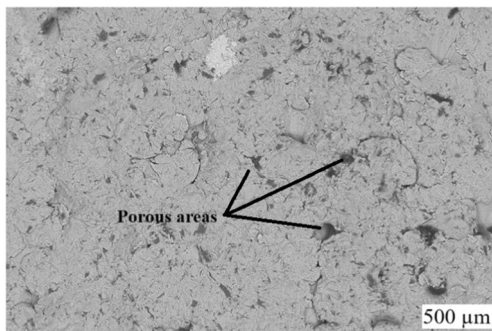


Fig. 5 Porous areas at the surface of the as-build SLM Ti6Al4V

β matrix, providing excellent toughness and resistance to crack propagation [32]. The equiaxed structure, composed of fine, uniformly distributed α and β grains, promotes isotropic mechanical properties and is often preferred for its superior fatigue performance [33]. In SLM, the rapid cooling rates promote the formation of a martensitic α' phase, leading to higher strength and hardness but often at the expense of ductility due to defects such as porosity and unmelted particles. Understanding these microstructures and their formation mechanisms is crucial for tailoring the mechanical properties of titanium alloys for specific applications. Furthermore, Mainly, in the SLM processing of Ti6Al4V4, two primary defect types prevail balling and unintended porosity. Because of the complete melting process employed, SLM is susceptible to instability in the melt pool, which, when combined with inadequately selected process parameters, may lead to the formation of microstructural defects and porosity [11, 34].

Vickers hardness assessments for the SLM and conventional material were conducted with a 10 kgf and 20 kgf loads and a 12.4 s dwell time, employing a Zwick/Roell Indentec testing device. Figure 1 shows the calibration, which is magnification at $\times 10$. A hardness profile was generated for every sample with multiple measurements spanning

from the top to the bottom of the specimen. The measurements maintained 0.3 mm from the sample surface to the center of the initial indentation. The region impression section shown in Fig. 6 defines the sample area where hardness analyses were conducted.

2.4 Details of the machining parameters

The work materials were evaluated for machinability using the face-turning method, a test designed specifically to assess the machinability of SLM and Conventional Ti6Al4V materials. The machining test involved three cutting speeds (mm/min), commencing at V_c 40 m/min, 80 m/min, and then 120 m/min. A constant feed rate (f) of 0.02 mm/rev and a depth of cut (d) of 0.5 mm were maintained throughout the test. The specifics of the machining trials are outlined in Table 4. Face-turning tests were conducted for designated machining durations, as indicated in Table 4.

The experiments were concluded after these machining passes, and the relevant data was documented. Face milling trials were conducted on the ecoMill 635 V, utilizing a carbide tool specifically designed for the machining center, as illustrated in Fig. 7a and b.

2.5 Details of the machinability test

Face milling experiments were conducted on the ecoMill 635 V machining center. The cutting tool details are illustrated in Fig. 7b. Cutting parameters were determined according to the tool manufacturer's specifications. Cutting forces were measured during each test using a Kistler Type 5697-DAQ dynamometer attached to the cutting tool (see Fig. 8). The dynamometer was linked to a Kistler 5697 multichannel charge amplifier.

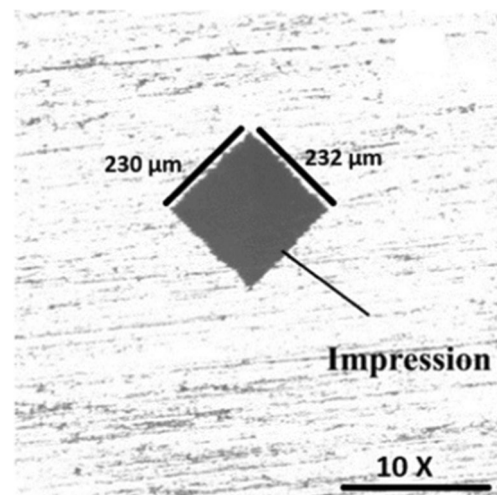


Fig. 6 Indentation impression for hardness test

Fig. 7 **a** Used milling machine and **b** carbide cutting tool

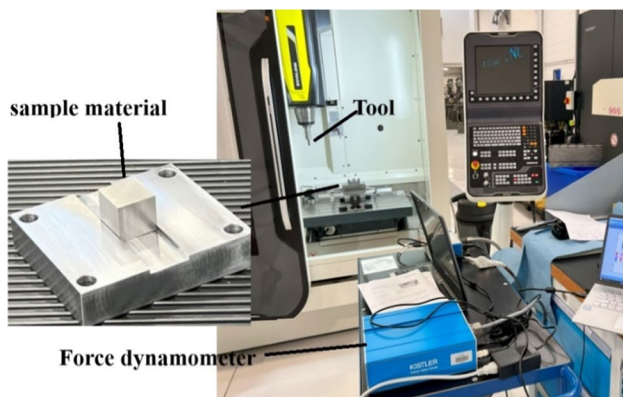
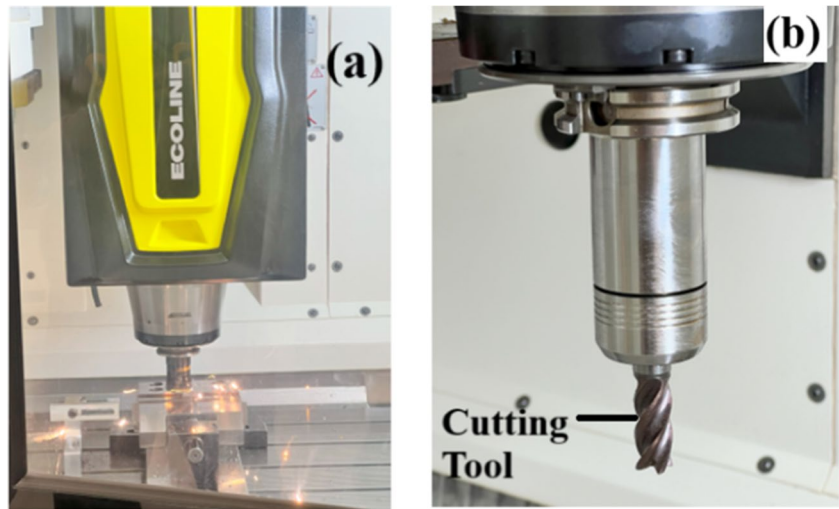


Fig. 8 ecoMill 635 V machining center and Kistler Type 5697-DAQ dynamometer

Table 4 Machining trails outlined as

Cutting conditions	Depth of cut (d)	Feed mm/rev
$V_c = 40$ m/min	0.5 mm	0.02
$V_c = 80$ m/min	0.5 mm	0.02
$V_c = 120$ m/min	0.5 mm	0.02

The milling test concluded when the cutting length covered the entire surface. The samples were secured in a Kistler dynamometer table, and the force-frequency spectra of the machining signals were examined. Cutting forces were recorded at a sample rate of 1000 and measuring time of 120 s. Additionally, the sample surfaces were examined through both optical and scanning electron microscopes. The surface roughness of the machined surface was assessed with a Contour X 200—Surface Measurement instrument, with three readings recorded at distinct locations and the mean value documented. Capturing secondary electron

images of the machined surface, a Hitachi tabletop microscope TM3030Plus was employed to analyze the surface characteristics.

3 Results and discussion

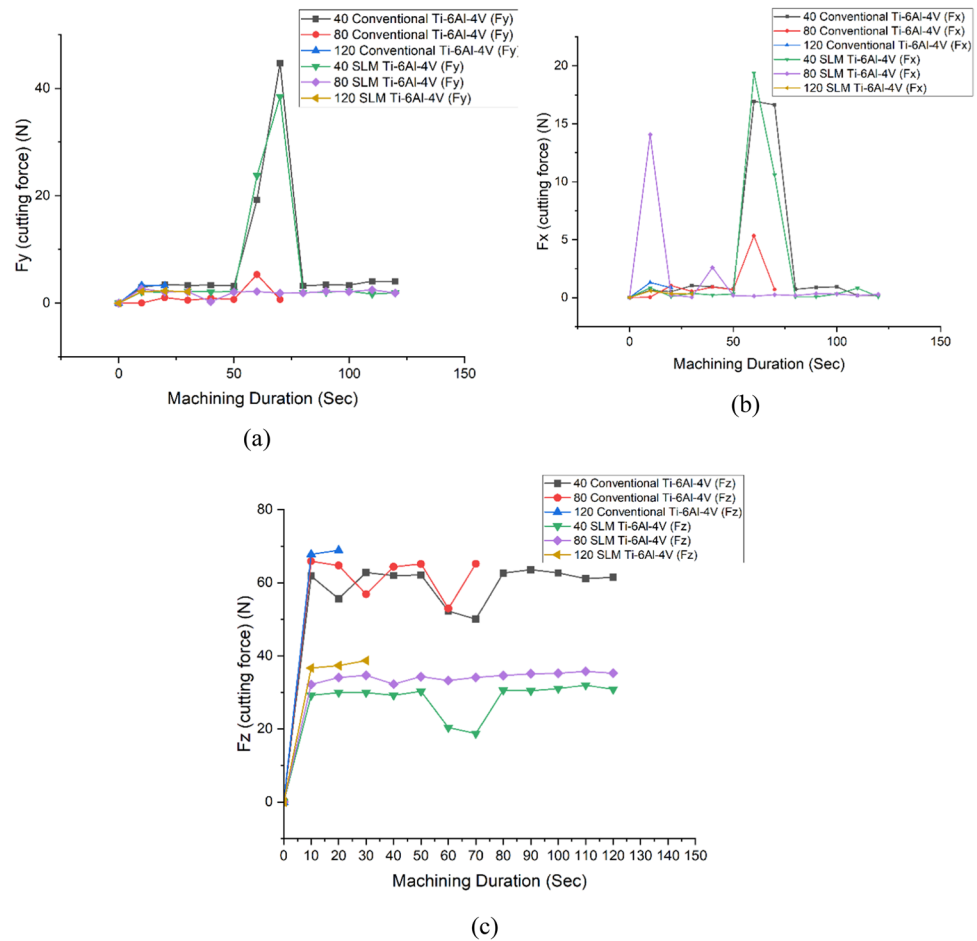
3.1 Cutting forces

The cutting forces demonstrated a robust connection with the material’s mechanical properties. The cutting forces generated at the tool’s cutting edge are pivotal parameters in evaluating the machinability of a material [35]. Additionally, understanding the interplay between cutting speed and force generation is essential for optimizing machining parameters. Figure 9 illustrates the average cutting force measured across all experimental trials throughout the machining process. During the process of material removal, the tool tooth is subjected to an instantaneous tangential force (F_t), instantaneous radial force (F_r), and instantaneous axial force (F_a) within the cutter system. Once the F_t , F_r , and F_a cutting forces are determined at the point of contact between the tooth and workpiece, the milling undergoes three force components: F_x , F_y , and F_z .

$$\text{The } F = \sqrt{F_x^2 + F_y^2 + F_z^2} \tag{2}$$

F_x , F_y , and F_z denote the cutting force components in the coordinate system’s x , y , and z directions [36]. It is essential to highlight that the resultant cutting force (F_z) holds a dominant position among force components, approximately four times greater than both the feed force (F_x) and thrust force (F_y) individually. Consequently, our emphasis on the discussion of cutting forces centers on the cutting force (F_z), given that the variations in F_x and F_y align with the same pattern observed in F_z . However, the primary cutting force F_z , being

Fig. 9 Different cutting force components during the machining of conventional and SLM Ti-6Al-4 V, denoted as **a** F_y , **b** F_x , and **c** F_z



the most power-consuming and exerting the most significant impact on the milling process, is the critical focus of cutting force analysis. In a single cutting pass, lasting 40 s, a total of three passes were executed to remove the material layer, resulting in a cumulative cutting time of 120 s as recorded on the Kistler Type 5697-DAQ dynamometer to obtain the cutting forces. Figure 9 illustrates the representation of F_x , F_y , and F_z , revealing the dynamic forces acting on the end mill. Notably, it was observed that the maximum cutting forces were recorded at a cutting speed of 120 m/min. A substantial disparity in cutting forces was observed when machining conventional Ti-6Al-4 V and SLM Ti-6Al-4 V. This notable contrast in cutting forces can be attributed to porosity and thermal softening. Furthermore, the material under consideration, SLM Ti6Al4V, exhibited lower cutting forces.

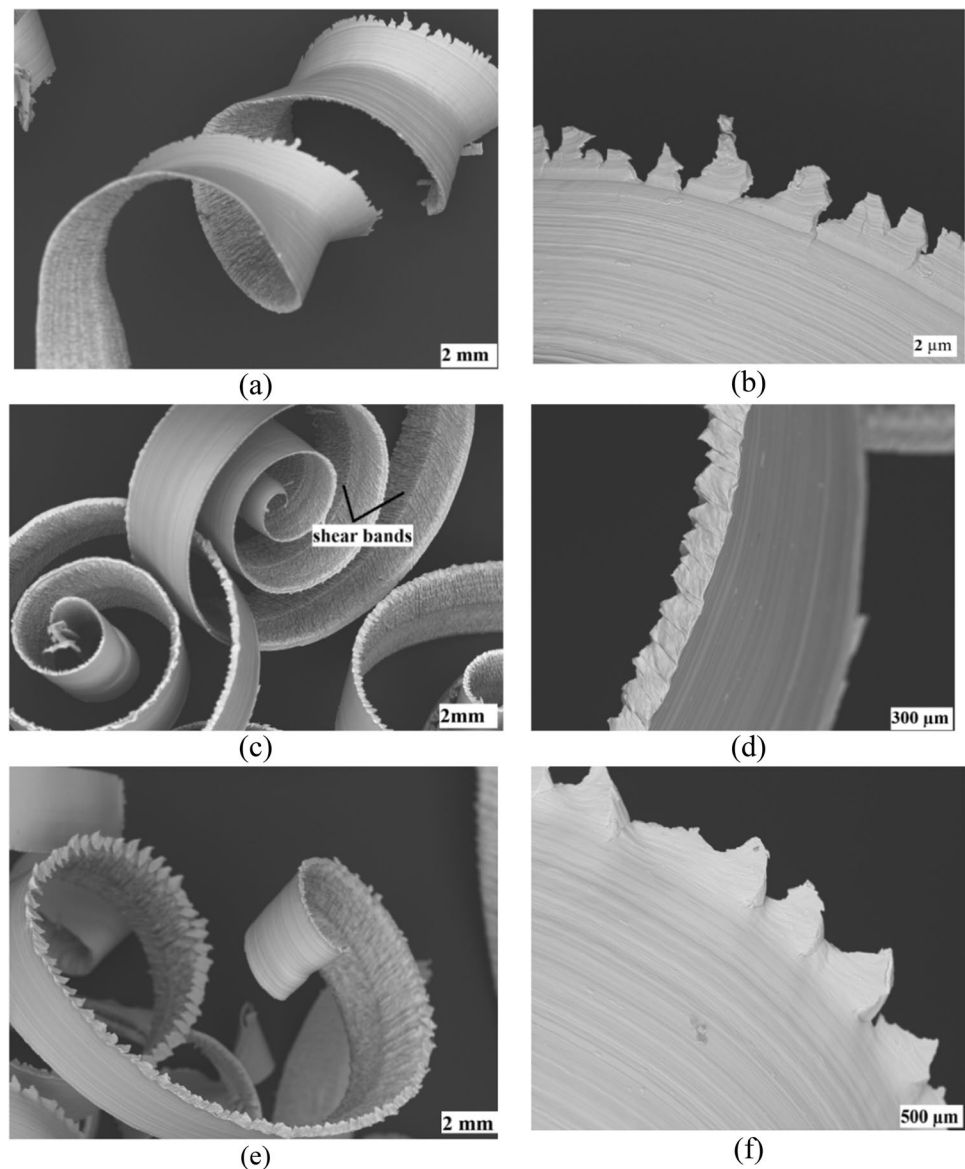
This phenomenon can be attributed to its inherent characteristics, including porosity and the presence of unmelted particles resulting from the SLM process. The porosity reduces material density, making it less resistant to the cutting tool. At the same time, the presence of unmelted particles influences the material's mechanical properties, contributing to smoother material removal and lower cutting

forces. In the case of SLM Ti6Al4V, the main cutting force (F_z) exhibits an initial rise followed by a decline as cutting speed increases. Ming et al. [21] stated that at elevated temperatures and high strain rates, SLM Ti6Al4V exhibits a more pronounced thermal-softening impact compared to its strain-hardening effect. It was observed that the plasticity of forged Ti6Al4V surpasses that of SLM Ti6Al4V. Notably, during milling, the plastic deformation of forged Ti6Al4V is more pronounced, and there is a heightened visibility of chip curling. Consequently, the machining process for forged Ti6Al4V demands more energy for chip formation, leading to a greater main cutting force than SLM Ti6Al4V. Consequently, when the cutting speed is set at 80 m/min, the axial force (F_z) for SLM Ti6Al4V decreases owing to the evident thermal-softening effect. In contrast, conventional Ti6Al4V displays a less noticeable thermal-softening effect at high strain rates than SLM Ti6Al4V. Therefore, as the cutting speed escalates to 80 m/min, there is an increase in F_z for conventional Ti6Al4V, but the rate of increase diminishes significantly. Additionally, F_z increases with higher feed per tooth and axial cutting depth. In contrast, for conventional Ti6Al4V, F_z rises with cutting speed, but the rate of increase diminishes at a cutting speed of 80 m/min.

Furthermore, F_z increases alongside higher feed per tooth and axial cutting depth. Furthermore, the minimal cutting forces observed in SLM Ti6Al4V indicate that the plasticity of conventional Ti6Al4V surpasses that of SLM Ti6Al4V. During the Milling of SLM Ti6Al4V a marginal rise in cutting force (8 N) occurred between 40 and 120 m/min, after which a consistent cutting force was maintained throughout the cutting speed. Notably, conventional Ti6Al4V exhibits more pronounced plastic deformation in the milling process, accompanied by a more conspicuous chip curling phenomenon (as depicted in Fig. 10). Consequently, the milling of conventional Ti6Al4V necessitates a greater energy for chip formation, leading to a higher main cutting force than SLM Ti6Al4V. As anticipated, SLM generally demonstrates heightened strength and hardness, characteristics that traditionally correlate with increased cutting forces. However,

contrary to this potential, SLM exhibited reduced cutting forces. This finding aligns with previous research on the milling of titanium alloy, where materials with greater hardness typically resulted in diminished cutting forces. Moreover, several studies on SLM Ti6Al4V have reported lower cutting forces during milling operations [37, 38]. It mainly referred to a critical factor influencing surface finish, and overall machining efficiency. Similarly, Bonaiti et al. investigated the milling machinability of Ti6Al4V produced via AM and exhibited lower cutting forces, which they attributed to the high porosity levels [39]. Another significant study by Hojati et al., it was noted that milling operations on fully dense AM titanium yielded lower forces compared to conventional extruded titanium, despite the former's higher hardness. This behavior can be attributed to various factors, such as distinct phases and grain structures observed in each

Fig. 10 The chip formations of the conventional Ti6Al4V in three different material conditions, examined at cutting speeds of **a** and **b** 40 m/min, **c** and **d** 80 m/min, and **e** and **f** 120 m/min



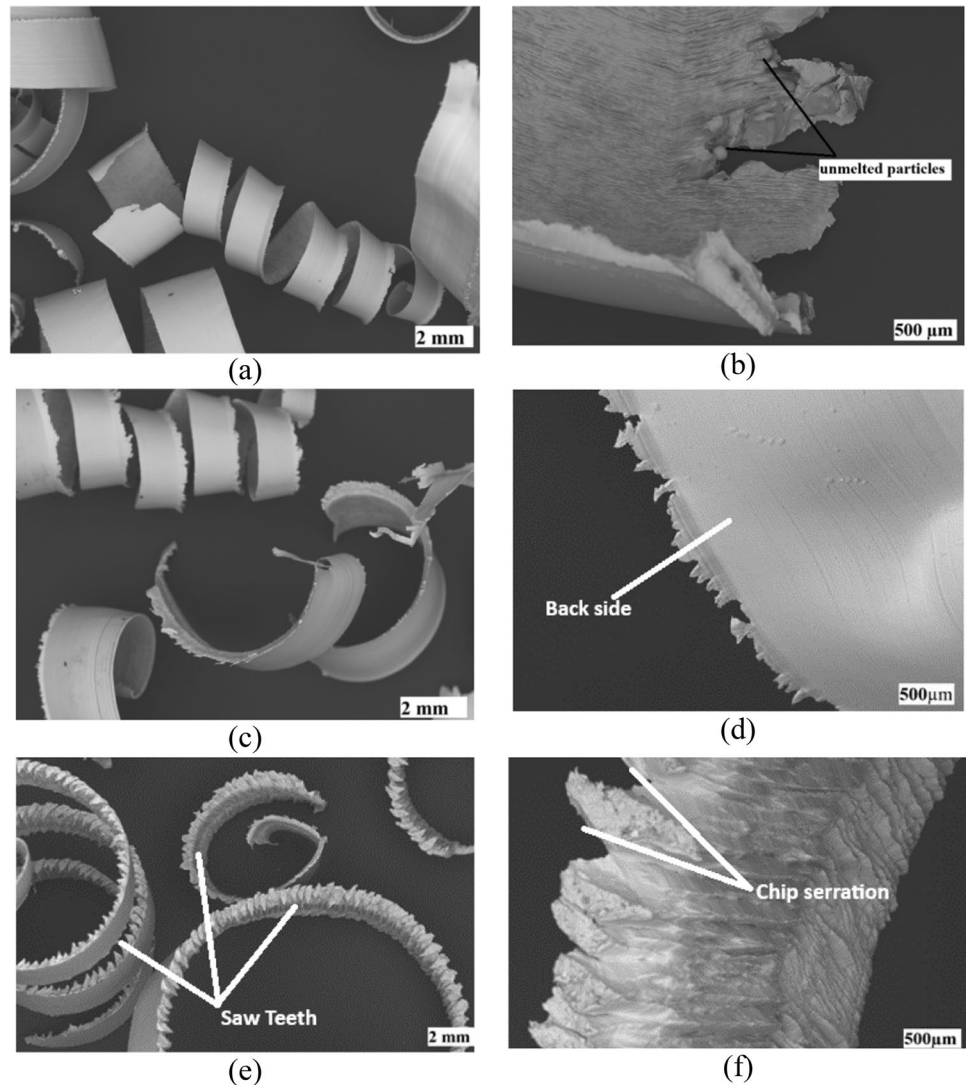
material. Specifically, the commercial alloy exhibited near-equiaxed alpha grains interspersed with alpha/beta regions, whereas the SLM sample revealed acicular alpha martensite embedded within an alpha matrix [40].

3.2 Chip analysis

Chip analysis involved studying the alterations in shape as the cutting length increased for each material and contrasting these changes with the shape modifications at the same cutting length under various material conditions. This section examined the chip formations of conventional and SLM as build Ti6Al4V under three distinct material conditions. The investigation is performed at cutting velocities of 40 m/min for conditions (a and b), 80 m/min for conditions (c and d), and 120 m/min for conditions (e and f), as illustrated in Figs. 10 and 11. No notable differences in the size and shape of the chips were discerned in either

scenario. It is established that titanium alloys generate segmented chips during machining [41, 42]. Figures 10 and 11 display images of the chips gathered in the third trial at cutting lengths of 20 m for conventional and as-build SLM Ti6Al4V. In Fig. 10, at 40 m/min (a and b), the chips are continuous with a uniform appearance. Shear bands are observed (Fig. 10c), indicating localized deformation. At 80 m/min (c and d), the chips show more significant segmentation and pronounced shear bands, highlighting the material's response to higher cutting speeds. At 120 m/min (e and f), the chips exhibit a distinct saw-tooth pattern, similar to SLM-produced chips but with less fragmentation. The SEM micrographs demonstrate that although all conditions produced segmented chips, the SLM chips showed slightly higher curling, suggesting accelerated chip flow due to reduced friction [43]. In Fig. 11, at a cutting speed of 40 m/min (a and b), the chips are continuous and ribbon-like, indicating a stable cutting process typical of

Fig. 11 The chip formations of SLM Ti6Al4V under three distinct material conditions, investigated at cutting speeds of **a** and **b** 40 m/min, **c** and **d** 80 m/min, and **e** and **f** 120 m/min



ductile materials. However, unmelted particles (Fig. 11b) are observed within the chips, a result of incomplete fusion during the SLM process. These unmelted particles can act as stress concentrators, compromising the mechanical properties of the machined part [44]. At 80 m/min (c and d), the chips become thinner and more fragmented, suggesting a transition towards segmented chips due to higher strain rates and thermal effects. The smooth backside of the chips (Fig. 11d) indicates effective shearing and efficient material removal, essential for achieving high-quality surface finishes [45]. At 120 m/min (e and f), the chips exhibit a saw-tooth pattern, reflecting a highly segmented nature due to thermal softening. The pronounced serrations (Fig. 11f) suggest localized deformation bands, a behavior commonly associated with high-speed machining, where increased temperatures facilitate chip segmentation [46]. The analysis revealed a discrepancy in chip thickness between the continuous segment and the segmented part, indicating a higher degree of slipping between the segments. Upon closer examination at higher magnification (Fig. 10b and e), distinctive deformation characteristics were observed during segmented and continuous chip formation. A continuous and uniform shearing process with a smaller slipping angle (35°) was identified during the continuous chip period. In contrast, a narrow shear band with more pronounced deformation and a larger slipping angle (50 to 55°) was observed in the sharp saw-tooth period. The regions where aperiodic saw-tooth chips formed exhibited shearing with smaller and larger slipping angles. The workpiece material's heterogeneous structure contributed to varying plastic deformability levels in different areas. Consequently, some regions displayed good plastic deformability at low cutting speeds, resulting in continuous chip formation (Fig. 10c) and static cutting forces. Certain regions, characterized by limited plastic deformability, cannot undergo deformation at this cutting speed. Consequently, this leads to the formation of segmented chips and the emergence of dynamic cutting forces (Fig. 9b). The initiation of segmented chip formation is contingent on the microstructure, determining the critical cutting speed. However, it is noteworthy that the shear band in the segmented chip remains independent of the microstructure. Additionally, Fig. 11b detected the unmelted powder particles dispersed throughout various sections of the chip, underscoring the practical implications of incomplete fusion during additive manufacturing, especially in processes like SLM. Gong et al. [44] stated that the insufficient energy input fundamentally gives rise to unmelted regions, forming pores and cracks and subsequently diminishing the material properties. This finding is particularly relevant in the assessment of material characteristics and performance. The identifying of these unmelted particles not only aligns with the anticipated

microstructural inhomogeneity but also provides a tangible manifestation of the potential consequences.

The material's susceptibility to elevated roughness, as indicated by the presence of these particles, stands as a concrete manifestation of the challenges associated with incomplete fusion. This observation adds a valuable layer to our chip analysis, emphasizing the need for meticulous attention to processing parameters. Additionally, it underscores the importance of implementing effective post-processing strategies to address and alleviate issues arising from unmelted particles, particularly during the machining of the final part.

This comprehensive approach ensures optimal material properties and performance in the product. Besides, the morphology of chips provides essential insights into the efficiency of the cutting process and the behavior of materials under varying conditions. Liu et al. observed that Ti6Al4V typically produces segmented or serrated chips due to its intrinsic properties, such as low thermal conductivity and high strength at elevated temperatures [47, 48]. A consistent observation was that chips from SLM Ti6Al4V parts exhibited more fragmentation and discontinuity compared to those from conventionally produced parts, aligning with the findings of Rubaie et al., as shown in Fig. 11 [43]. SEM micrographs showed that although all conditions produced segmented chips, SLM chips exhibited a slightly higher degree of curling. This increased curling suggests accelerated chip flow in the cutting zone due to reduced friction. The chip morphology of SLM-produced Ti6Al4V significantly influences cutting forces and anisotropy. During the machining of SLM-produced Ti6Al4V parts, cutting forces are more affected by the anisotropy introduced during the SLM process compared to conventionally produced parts [11, 45]. Fernandez-Zelaia et al. [49] revealed that cutting force sensitivity is influenced by the mechanical anisotropy of the part. Additionally, Ni et al. emphasized the evident connection between anisotropic cutting forces and the microstructure of SLM Ti-6Al-4 V samples [50]. This relationship is particularly significant given the diverse mechanical strength observed in different directions of SLM Ti6Al4V, resulting in variable cutting forces [51]. These findings highlight the intricate interplay between mechanical properties, cutting forces, and chip formation in the machining of SLM Ti6Al4V. In addition, a notable discrepancy in chip thickness between the continuous and segmented parts indicates a higher degree of slipping between segments. During continuous chip formation, a uniform shearing process with a smaller slipping angle (35°) is observed, while segmented chips show a larger slipping angle (50 to 55°), indicating more pronounced deformation. The initiation of segmented chip formation depends on the microstructure, determining the critical cutting speed. The shear band in segmented chips, however, remains independent of the microstructure. The heterogeneous structure of the workpiece material leads

to varying plastic deformability levels, causing continuous chip formation in regions with good plastic deformability at low cutting speeds and segmented chips in regions with limited deformability. These findings highlight the need for optimized machining parameters tailored to the specific microstructure and mechanical properties of SLM and conventional Ti6Al4V parts.

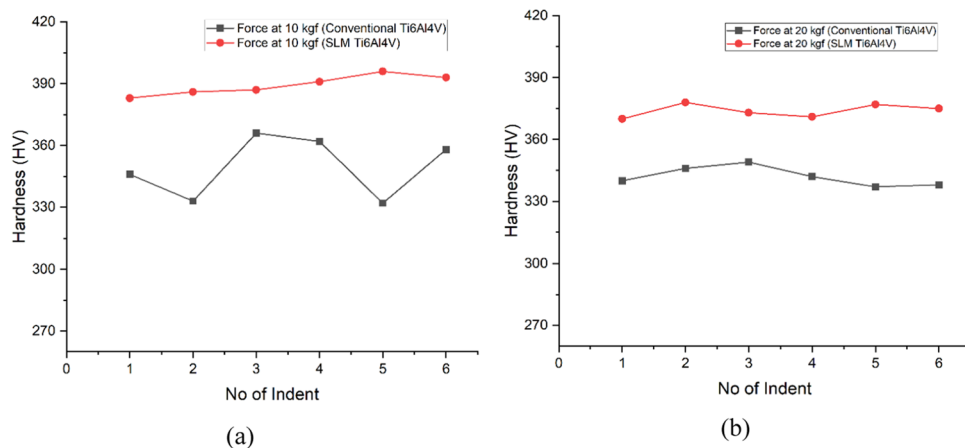
3.3 Hardness analysis

The hardness analysis section involved Vickers hardness assessments for SLM and conventional materials. The samples underwent machining to achieve a refined surface finish in preparation for the hardness analysis. Subsequently, emery paper was utilized to enhance the surface quality further. Following these preparation steps, Vickers hardness tests were conducted using a Zwick/Roell Indentec testing device, applying loads of 10 kgf and 20 kgf with a 12.4-s dwell time. A total of six indentations were systematically applied to each sample, both for conventional Ti-6Al-4 V and SLM Ti-6Al-4 V, to obtain a comprehensive set of values. Figure 12 shows the variations in Vickers hardness at different indentations under applied forces of (a) 10 kgf and (b) 20 kgf. In typical microstructures of $\alpha + \beta$ titanium alloys, various configurations such as Widmanstätten, duplex, basket-weave, and equiaxed structures are commonly observed. These microstructures play a crucial role in determining the mechanical properties of the alloys, including hardness [52]. Maharma et al. highlighted that in additive manufacturing and other alloy production processes, microstructural variations can be deliberately controlled or inadvertently influenced by processing parameters, facilitating the customization of material properties in research studies [53]. Furthermore, SLM can introduce distinctive microstructural characteristics like martensite phase regions, which notably affect both the hardness and mechanical strength of the material

[54]. Previously, Shunmugavel et al. [10] observed that components produced through the SLM process using Ti-6Al-4 V exhibit heightened yield strength, tensile strength, and hardness when compared to their conventional Ti-6Al-4 V counterparts. Similarly, as reported by Murr et al. [9], the increased strength and hardness observed in SLM Ti-6Al-4 V can be predominantly attributed to martensite phase regions in its microstructure. This unique microstructure and the existence of porosity contribute to a notable reduction in the ductility of SLM Ti-6Al-4 V compared to conventional Ti-6Al-4 V. Certainly.

However, the acquired results exhibited notable consistency with published findings. Particularly, noteworthy is the significantly higher hardness observed in SLM Ti-6Al-4 V compared to the conventional counterpart. The recorded hardness values were 390 (HV) under 10 kgf and 375 (HV) under 20 kgf applied forces, as illustrated in Fig. 12. These findings emphasize the strength and reliability of the hardness assessments, corroborating well with previously reported data. Additionally, these findings align with previous research by Thijs et al. which reported enhanced hardness in SLM-produced Ti-6Al-4 V [55]. Simonelli et al. also noted that the unique microstructure of SLM Ti-6Al-4 V, characterized by rapid cooling rates and associated phase transformations, contributes to increased hardness [56]. However, the presence of inherent porosity in SLM materials results in reduced ductility compared to conventionally manufactured Ti-6Al-4 V [28, 57]. These observations underscore the critical impact of SLM printing parameters on the mechanical properties of Ti-6Al-4 V. The ability to control and optimize these parameters allows for the tailoring of material properties to meet specific application requirements. This study confirms the reliability and consistency of Vickers hardness assessments, supporting the potential for SLM in producing high-performance Ti-6Al-4 V components.

Fig. 12 Illustrates the variation in Vicker hardness at different indentations under applied forces of **a** 10 kgf and **b** 20 kgf



3.4 Surface roughness

The surface roughness of the machined surface was evaluated using a Contour X 200 optical surface profilometer. The assessment of surface roughness was systematically conducted at multiple locations, as depicted in Fig. 13. This underscores the significance of machining in optimizing the quality of as-built SLM Ti6Al4V components. Variations in as-built roughness values were evident among SLM samples produced in three orientations (as referred in Fig. 13). Despite the utilization of reduced laser scan velocities to improve surface finish, as illustrated in Fig. 14, the average height of the selected surface (Sa) remained within the range of 3–5 μm in the as-built state. Additionally, the maximum height of the selected area (Sz) fell within 20–50 μm range. The outcomes of these measurements are graphically presented in Fig. 15, providing a comprehensive representation of the diverse surface characteristics observed at different points.

According to Yadroitsev et al. [58], surfaces in additive manufactured components often face challenges such as uneven layer delamination, powder distribution, and rippling effects caused by the laser's shear force on liquefied powder particles. Additionally, Shunmugavel et al. [59] proposed that addressing these issues and enhancing the surface quality of additive manufactured components invariably requires a finishing machining step. Consequently, the surface finishing of SLM-fabricated samples is essential to assess the quality of the as-built samples. Milton et al. [60] also explored the SLM specimens that pronounced anisotropy in cutting force, machined surface roughness, and work hardening. Meanwhile, the root means square values for all samples

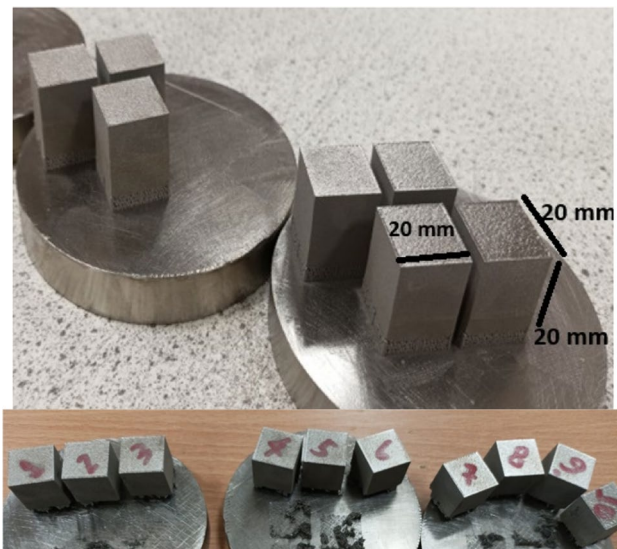


Fig. 13 As-built samples of SLM Ti6Al4V for a systematic assessment of surface roughness

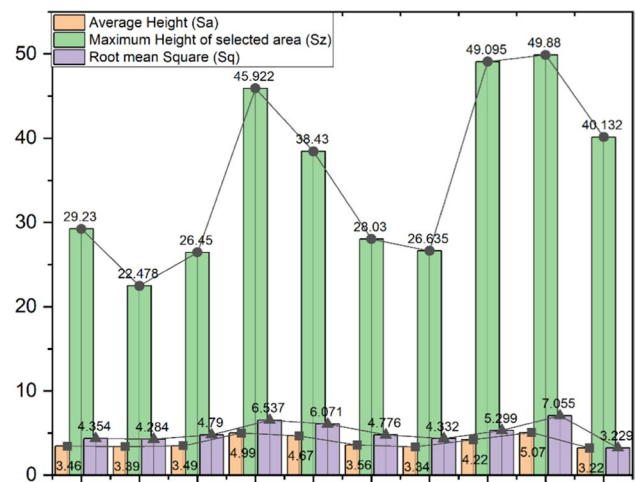


Fig. 14 illustrates the as-manufactured surface roughness of SLM samples on the uppermost surface

exhibited roughness within the 3–7 μm range. Expanding on the surface roughness section, it is noteworthy to emphasize findings consistent with Milton et al. in the literature, asserting that SLM samples demonstrated lower Ra values than conventional Ti6Al4V. This observation reinforces the efficacy of SLM in achieving superior surface quality, as further supported by the Sa, Sz, and root mean square measurements within specified ranges. The analysis of surface roughness for conventional Ti6Al4V reveals a relatively smoother profile compared to SLM Ti6Al4V. Conventional Ti6Al4V surfaces exhibit moderate roughness, with height variations predominantly between $-10 \mu\text{m}$ to $+70 \mu\text{m}$, as shown in Fig. 16. In contrast, SLM Ti6Al4V typically presents higher surface roughness due to the layer-by-layer build process, which introduces stair-stepping effects and residual powder particles, leading to higher roughness values [61].

Despite the complexity and material efficiency benefits of SLM, its inherent rougher surfaces pose challenges for applications requiring high precision and smooth finishes [62]. Hence, while SLM offers significant advantages in design flexibility and material utilization, conventional manufacturing methods remain superior in achieving smoother surface finishes essential for critical applications.

4 Conclusion

This study explores the Machining Characteristics of Titanium Alloy Components produced via Selective Laser Melting of Ti6Al4V. Milling tests were conducted on both conventionally and additively manufactured Ti-6Al-4 V. The machinability of these materials was thoroughly examined and compared at various speeds, considering aspects such as cutting forces, Chip analysis, hardness, and surface

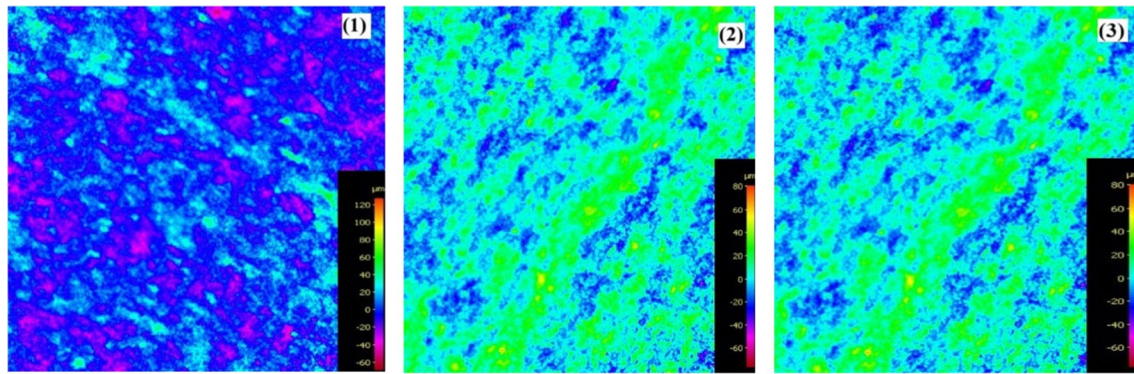


Fig. 15 Scan images from Contour X 200 showcasing the 3D topography of the SLM samples

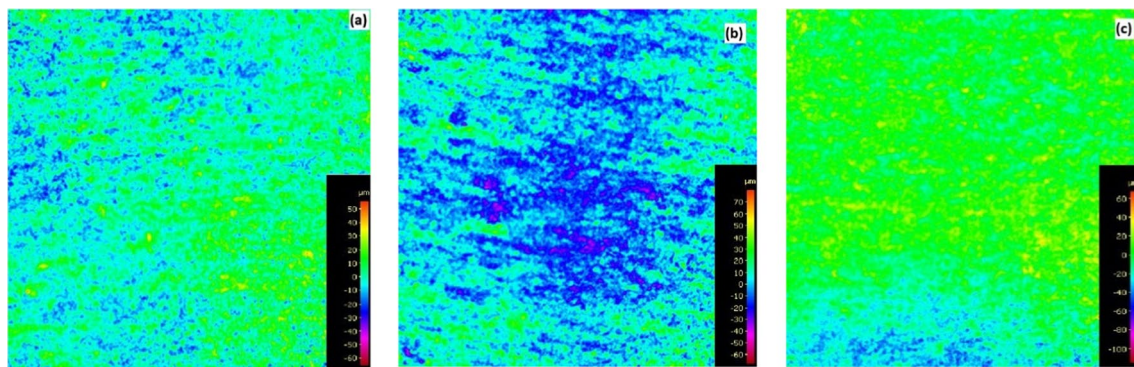


Fig. 16 Presents scan images obtained from Contour X 200, illustrating the 3D topography of the standard Ti6Al4V samples as shown in (a), (b), and (c)

roughness. Moreover, the investigation also centered on machinability, aiming to validate whether the material processing route influences machining behavior. The key findings can be encapsulated as follows:

- (i) As build SLM Ti6Al4V material exhibits lower cutting forces due to inherent characteristics, including porosity and the presence of unmelted particles resulting from the SLM process. The porosity reduces material density, making it less resistant to the cutting tool. At the same time, the presence of unmelted particles influences the material's mechanical properties, contributing to smoother material removal and lower cutting forces.
- (ii) Identifying of dispersed unmelted powder particles within the cutting chips of as-built SLM Ti6Al4V underscores the real-world consequences associated with incomplete fusion during additive manufacturing processes.
- (iii) Hardness of build SLM Ti6Al4V shows consistent and significantly higher hardness in SLM Ti-6Al-4 V compared to the conventional counterpart, with values of 390 (HV) and 375 (HV) under 10 kgf and 20

kgf, respectively. These findings affirm the reliability of hardness assessments.

- (iv) The as-built surface roughness of the selected area in SLM Ti6Al4V consistently falls within the 3–5 μm range. These findings underscore the reliability and replicability of the recorded roughness values, affirming that the SLM process consistently delivers a uniform surface finish within the defined specifications.

5 Future scope

The future scope involves integrating advanced techniques such as EBSD and Pole diagrams to analyze the microstructural characteristics and anisotropy of SLM Ti6Al4V alloys. This direction promises to enrich the understanding of machining properties and establish a comprehensive relationship between microstructure and machining behavior. Exploring the effects of various additive manufacturing parameters on these microstructural features could potentially optimize SLM processes, particularly for titanium alloys.

Acknowledgements We would like to express our gratitude for the support received from Atlantic Technological University Ireland in conducting this research.

Declarations

Conflict of interest The authors declare no competing interests.

References

- Pavithran NR, Harichandran R, Kumar DV (2023) Effect of Ytria-stabilized zirconia coating on the corrosion and thermal behaviour of additive manufactured Inconel 718 alloy. *J Alloy Compd* 968:171877
- Wang H, Li B, Zhang W, Xuan F (2023) Microstructural feature-driven machine learning for predicting mechanical tensile strength of laser powder bed fusion (L-PBF) additively manufactured Ti6Al4V alloy. *Eng Fract Mech* 295:109788
- Banerjee D, Williams JC (2013) Perspectives on titanium science and technology. *Acta Mater* 61(3):844–879
- Shunmugavel M, Polishetty A, Nomani J, Goldberg M, Littlefair G (2016) Metallurgical and machinability characteristics of wrought and selective laser melted Ti-6Al-4V. *J Metall Alloys* 3(1):9–12
- Brandt M (ed) (2016) *Laser additive manufacturing: materials, design, technologies, and applications*, 1st edn. Woodlands Publishing
- Shipley H, McDonnell D, Culleton M, Coull R, Lupoi R, O'Donnell G, Trimble D (2018) Optimisation of process parameters to address fundamental challenges during selective laser melting of Ti-6Al-4V: a review. *Int J Mach Tools Manuf* 128:1–20
- Ezugwu EO, Wang ZM (1997) Titanium alloys and their machinability—a review. *J Mater Process Technol* 68(3):262–274
- Bodziak S, Al-Rubaie KS, Dalla Valentina L, Lafratta FH, Santos EC, Zanatta AM, Chen Y (2019) Precipitation in 300 grade maraging steel built by selective laser melting: aging at 510 C for 2 h. *Mater Charact* 151:73–83
- Murr LE, Esquivel EV, Quinones SA, Gaytan SM, Lopez MI, Martinez EY, Wicker RB (2009) Microstructures and mechanical properties of electron beam-rapid manufactured Ti-6Al-4V biomedical prototypes compared to wrought Ti-6Al-4V. *Mater Charact* 60(2):96–105
- Shunmugavel M, Polishetty A, Littlefair G (2015) Microstructure and mechanical properties of wrought and additive manufactured Ti-6Al-4 V cylindrical bars. *Procedia Technol* 20:231–236
- Murr LE, Quinones SA, Gaytan SM, Lopez MI, Rodela A, Martinez EY, Wicker RB (2009) Microstructure and mechanical behavior of Ti-6Al-4V produced by rapid-layer manufacturing, for biomedical applications. *J Mech Behav Biomed Mater* 2(1):20–32
- Cabanettes F, Joubert A, Chardon G, Dumas V, Rech J, Grosjean C, Dimkovski Z (2018) Topography of as built surfaces generated in metal additive manufacturing: a multi scale analysis from form to roughness. *Precis Eng* 52:249–265
- Chen Z, Wu X, Tomus D, Davies CH (2018) Surface roughness of selective laser melted Ti-6Al-4V alloy components. *Addit Manuf* 21:91–103
- Oyelola O, Crawforth P, M'Saoubi R, Clare AT (2018) On the machinability of directed energy deposited Ti6Al4V. *Addit Manuf* 19:39–50
- Oyelola O, Crawforth P, M'Saoubi R, Clare AT (2018) Machining of functionally graded Ti6Al4V/WC produced by directed energy deposition. *Addit Manuf* 24:20–29
- Wang S, Zhu L, Fuh JYH, Zhang H, Yan W (2020) Multi-physics modeling and Gaussian process regression analysis of cladding track geometry for direct energy deposition. *Opt Lasers Eng* 127:105950
- Liu S, Shin YC (2019) Additive manufacturing of Ti6Al4V alloy: a review. *Mater Des* 164:107552
- Montevocchi F, Grossi N, Takagi H, Scippa A, Sasahara H, Campatelli G (2016) Cutting forces analysis in additive manufactured AISI H13 alloy. *Procedia Cirp* 46:476–479
- Oyelola O, Crawforth P, M'Saoubi R, Clare AT (2016) Machining of additively manufactured parts: implications for surface integrity. *Procedia Cirp* 45:119–122
- Armendia M, Osborne P, Garay A, Belloso J, Turner S, Arrazola PJ (2012) Influence of heat treatment on the machinability of titanium alloys. *Mater Manuf Processes* 27(4):457–461
- Ming W, Chen J, An Q, Chen M (2019) Dynamic mechanical properties and machinability characteristics of selective laser melted and forged Ti6Al4V. *J Mater Process Technol* 271:284–292
- Wysocki B, Maj P, Krawczyńska A, Roźniatowski K, Zdunek J, Kurzydowski KJ, Świążkowski W (2017) Microstructure and mechanical properties investigation of CP titanium processed by selective laser melting (SLM). *J Mater Process Technol* 241:13–23
- Duro M, Silva T, Marques MJ, Batista A, Rosa P, de Jesus A (2023) Influence of post-processing milling conditions on the machinability and residual stresses evolution of LPBF 18Ni300 maraging steel. *Int J Adv Manuf Technol* 127(5):2287–9
- Brinksmeier E, Levy G, Meyer D, Spierings AB (2010) Surface integrity of selective-laser-melted components. *CIRP Ann* 59(1):601–606
- Ezugwu EO, Bonney J, Yamane Y (2003) An overview of the machinability of aeroengine alloys. *J Mater Process Technol* 134(2):233–253
- Osakada K, Shiomi M (2006) Flexible manufacturing of metallic products by selective laser melting of powder. *Int J Mach Tools Manuf* 46(11):1188–1193
- Bordin A, Bruschi S, Ghiotti A, Bariani PF (2015) Analysis of tool wear in cryogenic machining of additive manufactured Ti6Al4V alloy. *Wear* 328:89–99
- Vrancken B, Thijs L, Kruth JP, Van Humbeeck J (2012) Heat treatment of Ti6Al4V produced by selective laser melting: microstructure and mechanical properties. *J Alloy Compd* 541:177–185
- Nguyen HD, Pramanik A, Basak AK, Dong Y, Prakash C, Deb Nath S, Buddhi D (2022) A critical review on additive manufacturing of Ti-6Al-4V alloy: microstructure and mechanical properties. *J Mater Res Technol* 18:4641–4661
- Ren XP, Li HQ, Guo H, Shen FL, Qin CX, Zhao ET, Fang XY (2021) A comparative study on mechanical properties of Ti-6Al-4V alloy processed by additive manufacturing vs traditional processing. *Mater Sci Eng A* 817:141384
- Samar SH (2019) Characterization of powder and bulk Ti-6Al-4V samples produced by electron beam melting process (Doctoral dissertation, Politecnico di Torino)
- Sk MB (2022) Heat treatment and effect of microstructural constituents on impact toughness of low carbon steel (Doctoral dissertation, Indian Institute of Technology Kharagpur)
- Liu Y, Wang F, Xu D, Wang J, Jiang F, Zarinejad M, Tong Y (2023) Microstructure and mechanical properties of laser metal deposited Ti6Al4V alloy with near equiaxed β grain structure. *J Market Res* 22:1935–1947
- Leuders S, Thöne M, Riemer A, Niendorf T, Tröster T, Richard HA, Maier HJ (2013) On the mechanical behaviour of titanium alloy TiAl6V4 manufactured by selective laser melting: fatigue resistance and crack growth performance. *Int J Fatigue* 48:300–307

35. Shunmugavel M, Polishetty A, Goldberg M, Singh R, Littlefair G (2017) A comparative study of mechanical properties and machinability of wrought and additive manufactured (selective laser melting) titanium alloy–Ti-6Al-4V. *Rapid Prototyp J* 23(6):1051–1056
36. Çelik YH, Karabiyik A (2017) Effect of cutting parameters on machining surface and cutting tool in milling of Ti-6Al-4V alloy. NISCAIR-CSIR, India, pp 349–356
37. de Oliveira Campos F, Araujo AC, Munhoz ALJ, Kapoor SG (2020) The influence of additive manufacturing on the micromilling machinability of Ti6Al4V: a comparison of SLM and commercial workpieces. *J Manuf Process* 60:299–307
38. Su Y, Li L, Wang G (2022) Machinability performance and mechanism in milling of additive manufactured Ti6Al4V with polycrystalline diamond tool. *J Manuf Process* 75:1153–1161
39. Bonaiti G, Parenti P, Annoni M, Kapoor S (2017) Micro-milling machinability of DED additive titanium Ti-6Al-4V. *Proc Manuf* 10:497–509
40. Hojati F, Daneshi A, Soltani B, Azarhoushang B, Biermann D (2020) Study on machinability of additively manufactured and conventional titanium alloys in micro-milling process. *Precis Eng* 62:1–9
41. Liu H, Zhang J, Xu X, Zhao W (2018) Experimental study on fracture mechanism transformation in chip segmentation of Ti-6Al-4V alloys during high-speed machining. *J Mater Process Technol* 257:132–140
42. Sun S, Brandt M, Dargusch MS (2009) Characteristics of cutting forces and chip formation in machining of titanium alloys. *Int J Mach Tools Manuf* 49(7–8):561–568
43. Al-Rubaie KS, Melotti S, Rabelo A, Paiva JM, Elbestawi MA, Veldhuis SC (2020) Machinability of SLM-produced Ti6Al4V titanium alloy parts. *J Manuf Process* 57:768–786
44. Gong H, Rafi K, Gu H, Ram GJ, Starr T, Stucker B (2015) Influence of defects on mechanical properties of Ti-6Al-4 V components produced by selective laser melting and electron beam melting. *Mater Des* 86:545–554
45. Liu D, Ni C, Wang Y, Zhu L (2023) Review of serrated chip characteristics and formation mechanism from conventional to additively manufactured titanium alloys. *J Alloys Compounds* 172573
46. Yameogo D, Haddag B, Makich H, Nouari M (2017) Prediction of the cutting forces and chip morphology when machining the Ti6Al4V alloy using a microstructural coupled model. *Procedia Cirp* 58:335–340
47. Mabrouki T, Courbon C, Zhang Y, Rech J, Nélis D, Asad M, Salvatore F (2016) Some insights on the modelling of chip formation and its morphology during metal cutting operations. *Comptes Rendus. Mécanique* 344(4–5):335–354
48. Zheng Z, Jin X, Bai Y, Yang Y, Ni C, Lu WF, Wang H (2022) Microstructure and anisotropic mechanical properties of selective laser melted Ti6Al4V alloy under different scanning strategies. *Mater Sci Eng A* 831:142236
49. Fernandez-Zelaia P, Nguyen V, Zhang H, Kumar A, Melkote SN (2019) The effects of material anisotropy on secondary processing of additively manufactured CoCrMo. *Addit Manuf* 29:100764
50. Ni C, Zhu L, Zheng Z, Zhang J, Yang Y, Yang J, Wang H (2020) Effect of material anisotropy on ultra-precision machining of Ti-6Al-4V alloy fabricated by selective laser melting. *J Alloys Compounds* 848:156457
51. Milton S, Rigo O, LeCorre S, Morandau A, Siriki R, Bocher P, Leroy R (2021) Microstructure effects on the machinability behaviour of Ti6Al4V produced by Selective Laser Melting and Electron Beam Melting process. *Mater Sci Eng A* 823:141773
52. Xu J, Zhu J, Fan J, Zhou Q, Peng Y, Guo S (2019) Microstructure and mechanical properties of Ti-6Al-4V alloy fabricated using electron beam freeform fabrication. *Vacuum* 167:364–373
53. Xu Y, Zhang D, Guo Y, Hu S, Wu X, Jiang Y (2020) Microstructural tailoring of As-Selective Laser Melted Ti6Al4V alloy for high mechanical properties. *J Alloy Compd* 816:152536
54. Shunmugavel M, Polishetty A, Goldberg M, Nomani J, Littlefair G (2017) Influence of build orientation on machinability of selective laser melted titanium alloy-Ti-6Al-4V. *Int J Mater Metallurg Eng* 11(8):523–527
55. Thijs L, Verhaeghe F, Craeghs T, Van Humbeeck J, Kruth JP (2010) A study of the microstructural evolution during selective laser melting of Ti-6Al-4V. *Acta Mater* 58(9):3303–3312
56. Simonelli M, Tse YY, Tuck C (2012) Microstructure of Ti-6Al-4V produced by selective laser melting. In *Journal of Physics: Conference Series* (Vol. 371, No. 1, p. 012084). IOP Publishing
57. Gong H, Rafi K, Gu H, Starr T, Stucker B (2014) Analysis of defect generation in Ti-6Al-4V parts made using powder bed fusion additive manufacturing processes. *Addit Manuf* 1:87–98
58. Yadroitsev I, Smurov I (2011) Surface morphology in selective laser melting of metal powders. *Phys Procedia* 12:264–270
59. Shunmugavel M, Polishetty A, Goldberg M, Singh RP, Littlefair G (2016) Tool wear and surface integrity analysis of machined heat treated selective laser melted Ti-6Al-4V. *Int J Mater Form Mach Process* 3(2):50–63
60. Milton S, Morandau A, Chalon F, Leroy R (2016) Influence of finish machining on the surface integrity of Ti6Al4V produced by selective laser melting. *Procedia Cirp* 45:127–130
61. Trithpechunlayakoon S, Soe AN, Sombatmai A, Khruaduangkham S, Trachoo V, Promopattum P, Srimaneepong V (n.d.) The analysis of different void morphology related to mechanical properties of L-Pbf Ti-6al-4v Eli alloy influenced by laser energy density for biomedical applications. Available at SSRN 4631939
62. Hashmi AW, Mali HS, Meena A (2023) Improving the surface characteristics of additively manufactured parts: a review. *Mater Today Proc* 81:723–738

Publisher's Note Springer Nature remains neutral with regard to jurisdictional claims in published maps and institutional affiliations.

Springer Nature or its licensor (e.g. a society or other partner) holds exclusive rights to this article under a publishing agreement with the author(s) or other rightsholder(s); author self-archiving of the accepted manuscript version of this article is solely governed by the terms of such publishing agreement and applicable law.